applied sciences

MDPI

Article

Analytical Study on the Low-Frequency Vibrations Isolation System for Vehicle's Seats Using Quasi-Zero-Stiffness Isolator

Mohammad Abuabiah [1,*], Yazan Dabbas [1], Luqman Herzallah [1], Ihab H. Alsurakji [1], Mahmoud Assad [1] and Peter Plapper [2]

[1] Mechanical and Mechatronics Engineering Department, Faculty of Engineering and Information Technology, An-Najah National University, Nablus P.O. Box 7, Palestine; yazan.dabbas@stu.najah.edu (Y.D.); luqman.h@najah.edu (L.H.); isurakji@najah.edu (I.H.A.); m_assad@najah.edu (M.A.)

[2] Department of Engineering, University of Luxembourg, 6, rue-Kalergi, L-1359 Luxembourg, Luxembourg; peter.plapper@uni.lu

* Correspondence: m.abuabiah@najah.edu

Featured Application: Vibration Isolation System for Vehicle's Seats.

Abstract: Improving the vibration isolation for the seat of small vehicles under low excitation frequencies is important for providing good comfort for the driver and passengers. Thus, in this study, a compact, low-dynamic, and high-static stiffness vibration isolation system has been designed. A theoretical analysis of the proposed quasi-zero stiffness (QZS) isolator system for vehicle seats is presented. The isolator consists of two oblique springs and a vertical spring to support the load and to achieve quasi-zero stiffness at the equilibrium position. To support any additional load above the supported weight, a sleeve air spring is used. Furthermore, the two oblique springs are equipped with a horizontal adjustment mechanism that is aimed to reach higher frequencies with the existed stroke when a heavy load is applied. The proposed system can be fitted for small vehicles, especially for B-segment and C-segment cars. Finally, the simulation results reveal that the proposed system has a large isolation frequency range compared to that of the linear isolator.

Keywords: quasi-zero stiffness; vibration isolation; low-frequency; vehicle seat

check for updates

Citation: Abuabiah, M.; Dabbas, Y.; Herzallah, L.; Alsurakji, I.H.; Assad, M.; Plapper, P. Analytical Study on the Low-Frequency Vibrations Isolation System for Vehicle's Seats Using Quasi-Zero-Stiffness Isolator. *Appl. Sci.* **2022**, *12*, 2418. https://doi.org/10.3390/app12052418

Academic Editor: Xiao-Dong Yang

Received: 31 January 2022
Accepted: 22 February 2022
Published: 25 February 2022

Publisher's Note: MDPI stays neutral with regard to jurisdictional claims in published maps and institutional affiliations.

Copyright: © 2022 by the authors. Licensee MDPI, Basel, Switzerland. This article is an open access article distributed under the terms and conditions of the Creative Commons Attribution (CC BY) license (https://creativecommons.org/licenses/by/4.0/).

1. Introduction

Despite the massive evolution in the vibration isolation systems where cars, buses, and trucks were the main focus in road and off-road efforts until the present, they still lack the ability to provide complete comfort for drivers and passengers. Mechanical vibration is still one of the trickiest challenges that face engineers when it comes to achieving optimum comfort.

Many studies have shown that drivers are exposed to a decent level of body vibrations, e.g., [1,2]. Exposure to such high-intensity and low-frequency vibration may cause fatigue, low back pain, and discomfort, especially among long-haul drivers. Additional studies went a step further, more specifically studying the body's resonant frequency under different postural conditions, hand positions, seat heights, and back support conditions for healthy adults of different gender and ages [3–9]. The conclusions that can be drawn from the previous studies are that the resonant frequencies of the human body parts are between 4 and 17 Hz, and the average of the human body's resonant frequency is approximately 7 Hz, which means they fall into the range of the vibrations that occur at low frequency.

Over the past years, numerous studies have been dedicated to finding a solution to this problem. Gan et al. [10] designed a hybrid system that combines passive suspension and active actuators. The passive part consists of a conventional spring and damper to support the driver's weight and seat, whereas the active part is just two electromagnetic linear actuators controlled using a fully adaptive controller to achieve a decent isolation performance. Li et al. [11] developed a vibration isolator with a flywheel device as an essential

part. In this study, the authors take into account a non-ideal case that includes factors such as the mass of the structure, friction, and stiffness along with the ideal two-terminal mass. The study focused on passenger comfort, tire grip, and suspension deflection. Speaking of passive systems, a tuned mass damper for self-excited vibration control was recently introduced by Zhang et al. [12]. In contrast, Stein [13] proposed an active vibration isolator using a relief spring to maintain the weight and air spring controlled by a linear controller with an electro-pneumatic transducer as a sensing element. Similarly, Maciejewski et al. [14] proposed an active system consisting of a hydraulic damper and an air spring controlled by directional control valves and a controller with triple feedback loops. Ning et al. [15] designed an active vibration isolator by choosing two inexpensive rotary motors controlled by an H_∞ controller and a careful selection of the spring stiffness to reduce the resonant frequency of the seat as much as possible. The same authors of the previous study used the same controller but replaced the two rotary motors with a generator, which consisted of a regenerative shock absorber and an energy storage circuit used to store vibration energy in a battery [16]. Choi et al. [17] suggested a semi-active vibration isolator using a magnetorheological fluid damper, which is positioned at a certain angle and controlled by a skyhook controller. The previous studies [13–16] share a main and common part, which is so-called the scissor mechanism [18]. This type of machine is widely used in many fields, especially in isolation applications due to its capacity for heavy load-bearing and good equilibrium stability.

Permanent electromagnets, and magnet systems in general, attracted many researchers' attention in the last couple of years. Carrella et al. [19] proposed a high-static low-dynamic stiffness (HSLDS) vibration isolator using three magnets. Two of them are fixed on the edges, whereas the third one is located in the middle, which can move only in the vertical direction by sliding on a smooth vertical bar. The three magnets' attraction acts as a negative stiffness that opposes the conventional spring, which acts as a positive stiffness, thus, together they achieve zero or near-zero overall stiffness. Using a structural beam instead of a conventional spring as a positive stiffness part, Zhou [20] designed an electromagnetic vibration isolator that exhibits the HSLDS behaviour by controlling the amount of current delivered to the two electromagnets. Zheng et al. [21] proposed an HSLDS vibration isolator using two coaxial rings with opposite magnetization directions. This arrangement of negative stiffness magnetic spring (NSMS) along with a parallel mechanical spring can reduce the resonant frequency of the system, thus giving better isolation performance. Similarly, Dong et al. [22] used the same arrangement (NSMS) with a special design of spiral flexure spring (SFS) instead of the mechanical spring.

Another isolation system under the name of quasi-zero stiffness (QZS) has also been extensively investigated in the recent years, as an essential branch of the nonlinear vibration isolation systems. It exhibits a tremendous isolation performance if the system is well designed. Many studies have adopted this system using different ways of implementation to achieve what is so-called ultra-low frequency vibration isolation. Kovacic et al. [23] deeply studied the essential characteristics of the QZS vibration isolator and the static and dynamic analysis of a simple design. The QZS vibration system merely comprises a vertical spring and two oblique springs in a pre-stressed state considering the linear and nonlinear cases. Carrella et al. [24] have extended the research by studying the force transmissibility of each case and comparing them with a linear system. Instead of using simple oblique springs, many other negative stiffness structures have been proposed. Xu et al. [25] proposed a QZS vibration isolator consisting of a vertical linear spring and a unique negative stiffness structure using two magnets at each side with the same polarity. When the system is loaded, the linear spring is compressed, and the two magnets move closer to each other, which produces an immense repulsive force that keeps the system at an equilibrium position. Liu et al. [26] used two oblique Euler buckled beams as a negative stiffness structure. Upon adding this negative structure, the two-beam' endpoints are aligned in the horizontal equilibrium state, which gives zero summation forces, thus, a vertical spring reduces the system's resonant frequency to its minimum. Zhou et al. [27] developed a QZS vibration

isolator with unique mechanisms consisting of a fixed semi-circular cam sliding vertically on a roller that is connected to a horizontal spring by a slider. A vertical spring is connected to two adjusters that keep the system at the equilibrium position whatever the load is to achieve better isolation performance. Kim et al. [28] proposed a QZS vibration isolator using a negative structure consisting of a horizontal spring, flexures, a vertical spring, and a vertical compensator. The compensator is used to increase the linear spring's preload bearing capacity, whereas, the horizontal spring is used to apply compression force on the flexures to act as a whole as a negative structure while supporting a wide range of loads simultaneously.

Ahn et al. [29] designed a negative stiffness structure consisting of a sliding block connected with a horizontal spring coupled with an adjuster from one side and a bar hinged to the mass from the other side. Parallel with the negative structure, a pneumatic cylinder connected to a directional valve, where a neural network is used as a controller, a vertical spring, and a damper are selected to lower the overall stiffness and support a wide range of loads. Wie et al. [30] proposed a QZS vibration isolation system that uses scissor-like structures (SLSs), which are parts of the negative stiffness corrector along with a spring and a damper in each SLS. The scissor-like design consists of four connecting rods, where each pair is joined together and has the same length. Regarding the vertical components, a spring and a viscous damper are used in parallel with a linear guide to ensure that the movement is only in the vertical direction. Liao et al. [31] proposed a QZS vibration isolator with a generic negative stiffness structure that comprises a horizontal spring connected with an oblique rod on each side. However, in order to increase the performance of vibration isolation, an adjustable inert element attached to each oblique rod was implemented.

In this study, an alternative means of vibration isolation with the combination of a QZS isolator and an air spring is proposed for the car seat. The isolator is designed taking into consideration certain requirements, specifically, simplicity, compactness, and compatibility with different loads. To the best of the authors' knowledge, none of the previous studies have fulfilled these requirements nor developed such a mechanism for small vehicles, especially for B-segment and C-segment cars. Therefore, the novelty of this study is to design a system that can deal with the load variation with high isolation efficiency, simplicity, and compactness and could fit under the vehicle's seat. The paper is organized as follows. A fundamental review of the vibration isolation system is discussed in Section 2. The design method of the proposed vibration isolation system is discussed in Section 3. The numerical simulation results are shown in Section 4. Finally, Section 5 ends the paper with conclusions and remarks.

2. Fundamental Review on Vibration Isolation Systems

This section reviews the fundamental theory of vibration isolation systems and the key concepts of the QZS system.

A vibration system consists of an inertial element (which could be represented as a translating block having mass equal to m) and a restoring element (which could be represented by a coiled spring having stiffness equal to k). The system vibrates in response to initial conditions or to a force, or to both initial conditions and force. The restoring element exerts on the mass by a restoring force, such as spring force; $F_{spring} = kx$.

Many systems vibrate due to a force exerted on the inertial element, and this force may have different shapes; it may be harmonic, impulse, periodic, or random. In this study, the harmonic force is used to simulate the vibration source of the system. The reason to choose the harmonic force comes from the fact that this force is one of the most common forms of force represented in the road profile and can be easily analyzed in comparison to other types of forces [32]. Thus, the theory presented here is dedicated to solving the problems of harmonic excitation.

The equation of motion of a spring-mass system that is subjected to harmonic force has the following form:

$$m\ddot{x} + kx = F_0 \sin \omega t \tag{1}$$

where m is the equivalent mass of the system, k is the stiffness of the restoring element (spring), F_0 is the amplitude of the harmonic force, ω is the frequency of excitation, x is the position of the inertial element, and $\ddot{x}$ is the second derivative of the position of the inertial element in terms of the time, in other words, it is the acceleration of the inertial element.

The solution of the equation of motion consists of two parts: a homogeneous part and a complementary part. It can be expressed as

$$x(t) = A \sin \omega_n t + B \cos \omega_n t + X \sin \omega t \tag{2}$$

where ω_n is the natural frequency of the system, which depends on the specifications of the system itself, regardless of the type of the force, $\omega_n = \sqrt{\frac{k}{m}}$; X is the amplitude of the steady-state solution, which depends on the amplitude of the force, the natural frequency, and the excitation frequency; A and B are the amplitudes of the transient solution, which can be calculated with the aid of initial conditions.

The excitation may happen at the inertial element itself, which can be expressed by the equation of motion; the excitation may also be due to a force exerting on the base of the system.

2.1. Base Excitation

When the force exerts on the base of the system, it will lead to a deformation in the restoring element. This is different from the deformation when the force exerts on the inertial element itself because the deflection of the spring under base excitation will happen at its both ends, i.e., $F_{spring} = k(x - y)$. Here, x is the position of the inertial element, and y is the position of the base, which can be expressed by the following equation of motion:

$$m\ddot{x} + kx = ky \tag{3}$$

However, if the base moves in harmonic shape, the term y can be described as

$$y(t) = Y \sin \omega t \tag{4}$$

This leads to a similar equation to that of the forced system,

$$m\ddot{x} + kx = kY \sin \omega t \tag{5}$$

Therefore, the equation that describes the position of the inertial element will be

$$x(t) = A \sin \omega_n t + B \cos \omega_n t + X \sin \omega t \tag{6}$$

This is the same as Equation (2) except the term X, which now depends on the stiffness of the spring, the amplitude of the base motion, the natural frequency of the system, and the excitation frequency.

A useful study of vibration isolation is to determine the properties of the system that affect the transmission of vibration the most, which in this case happens to be the ratio between the natural frequency and the excitation frequency. It was observed that the maximum transmission of vibration happens when the ratio $r = \frac{\omega}{\omega_n} = 1$, and then the effect of vibration on the inertial element decays with the increment of r.

As a result, to isolate vibration, it is advised to reduce the natural frequency of the system, which could be done by increasing the mass of the system or decreasing the stiffness of the system. The first solution is not preferred for vehicles' manufacturers, because they tend to produce lighter vehicles than in the past. Hence, the solution that sounds more feasible is to reduce the stiffness of the system, which could be done in different ways. One

way to lower the stiffness of the system in order to isolate vibrations is to use the so-called Quasi-Zero- Stiffness system.

2.2. Quasi-Zero Stiffness System

The quasi-zero-stiffness (QZS) is a system where the stiffness approaches zero or stays around zero. Figure 1 shows a schematic sketch of one of the famous QZS systems, which consists of one vertical spring (k_p), and two oblique springs (k_n) that are inclined at a predetermined angle (θ_0) from equilibrium position (the QZS is in its originally undeformed position).

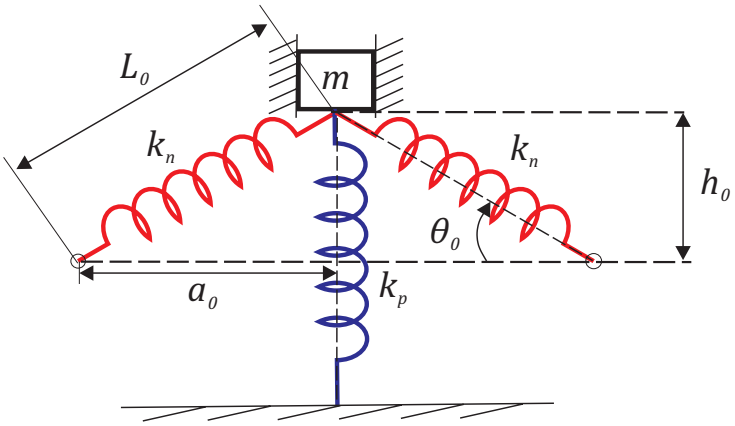


Figure 1. A simple model of the QZS system.

Figure 1 shows the QZS system at rest mode in its simplest form. However, such a design is vulnerable to many factors that may affect the range of stability around zero stiffness. These factors can be simply summarized in the geometrical factors and the stiffness ratio. The geometrical factors are the length of each spring (the oblique and vertical springs) and the inclination angle of the oblique springs. Putting all of these factors together helps in determining the distance between the suspension point of the oblique spring and the line of action of the vertical spring.

To achieve better control of the zero stiffness, it is advised to adjust the location of the horizontal deflection component for the oblique spring x_h with the help of either a manual adjuster or linear actuator, which is fitted at the suspension point of the oblique springs, as shown in Figure 2.

The factors that affect the range of stability of the QZS system are expressed as follows: geometric ratio $= \frac{a_0 - x_h}{2(L_0 - a_0 + x_h)}$ and the stiffness ratio $= \frac{k_n}{k_p}$.

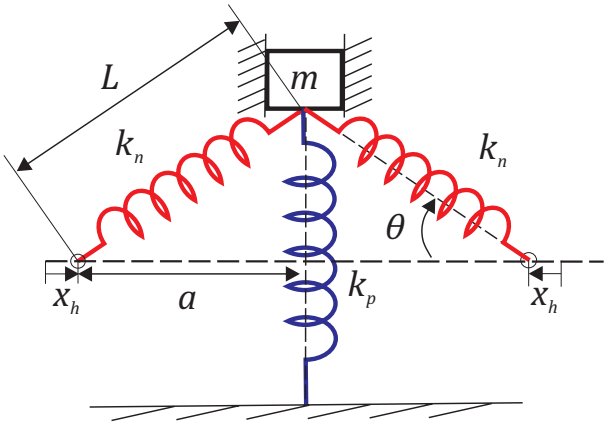


Figure 2. QZS system with the horizontal deflection.

3. Design Method for the Vibration Isolation System

The aim of this study is to design a compact system that fits beneath the seat of the driver to isolate harmful low frequency vibrations that are transmitted to the driver's body. The uniqueness of the proposed solution is the usage of a QZS system modified with an air spring. Figure 3 illustrates the proposed system schematic and it also shows that the source of vibration on the seat $x(t)$ is the motion of the base, which happens due to the irregularity of the road profile $d(t)$.

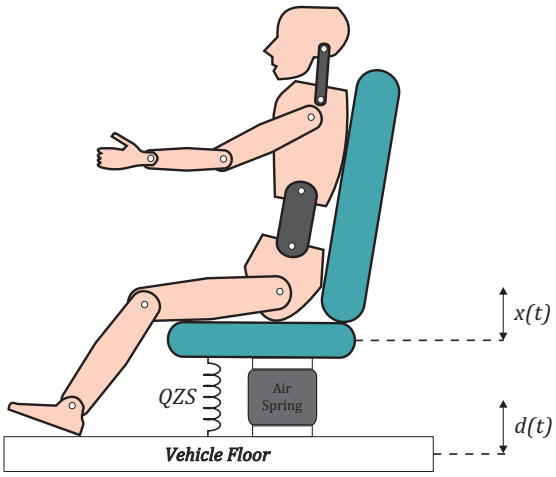


Figure 3. Dynamic model of the proposed system.

The equation of motion for the system shown in Figure 3 can be expressed as

$$m\ddot{x} + c(\dot{x} - \dot{d}) + F_{spring} = 0 \tag{7}$$

where c is the damping coefficient, and F_{spring} is the system spring force, given by

$$F_{spring} = \frac{k_n L_0}{(a_0 - x_h)^3}(x - d)^3 = \beta(x - d)^3 \tag{8}$$

where L_0 and a_0 are the free length of the oblique spring and horizontal distance, respectively. Equation (8) represents the approximated form of the force summation. The approximation is done using Taylor series expansion, as will be discussed in Section 3.1.

As mentioned earlier, $d(t)$ is considered to be a harmonic function, given by

$$d(t) = D \sin \omega t \tag{9}$$

Equations (8) and (9) can be used to rewrite the equation of motion as

$$\ddot{x} + 2\zeta\omega_n(\dot{x} - D\omega \cos \omega t) + \frac{\beta}{m}(x - D \sin \omega t)^3 = 0 \tag{10}$$

where ζ is the damping ratio, and the natural frequency of the system is expressed in the following form:

$$\omega_n = \sqrt{\frac{K}{m}} = \sqrt{\frac{3k_n L_0}{m(a_0 x_h)^3}|x|} \tag{11}$$

Hence, the natural frequency is variable due to the nature non-linearity of the system.

3.1. Static Analysis of the QZS System

The aim of the following analysis is to set the equilibrium position and to determine when the equivalent stiffness of the system is equal to zero. The equilibrium position is determined when the angle of inclination for the oblique springs is equal to zero. At

this equilibrium position and under a compression force acting on the slider mass (m), the vertical spring and the two oblique springs are compressed, as shown in Figure 4.

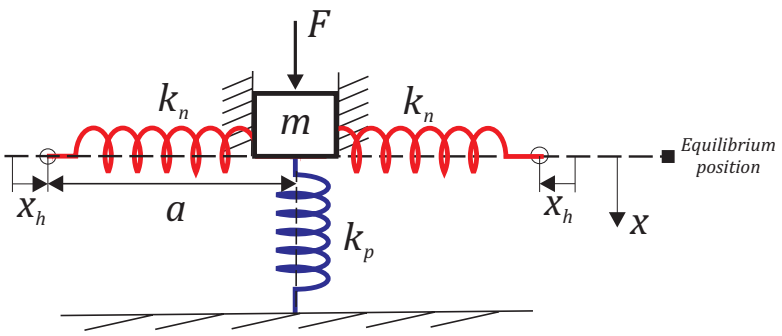


Figure 4. QZS system at equilibrium.

It is found that the summation of the forces acting on block m is

$$F = k_v(x + h_0) + 2k_n x(1 - \frac{L_0}{\sqrt{(a_0 - x_h)^2 + x^2}}) \tag{12}$$

where $k_v = k_p + k_{as}$, and k_{as} is the air-spring stiffness. It is worth noting that, in the situation where the applied force can be handled by the vertical spring alone, no air is delivered to the air spring and thus the vertical stiffness approximately equals k_p (see Sections 3.2 and 4.1 for more details). Conversely, when the force exceeds what the vertical spring can withstand to maintain equilibrium, this over-weight can be supported by the air spring, but at the expense of an increase in the stiffness. However, this poses no problem thanks to the presence of a horizontal-adjustment mechanism that can negate this situation by keeping the geometrical ratio and stiffness ratio equal.

At the equilibrium position, $x = 0$, Equation (12) reduces to

$$F = k_v h_0 \tag{13}$$

The equation below describes the equivalent stiffness of the system and is obtained by taking the derivative of the force F with respect to the deflection x, as follows:

$$K = k_v + 2k_n(1 - \frac{L_0(a_0 - x_h)^2}{[(a_0 - x_h)^2 + x^2]^{\frac{3}{2}}}) \tag{14}$$

Now, to determine the situation where the stiffness equals zero, simply substitute $K = 0$ and $X = 0$ in Equation (14). Hence, zero stiffness is achieved when the geometric ratio and the stiffness ratio are the same:

$$\frac{k_n}{k_p} = \frac{a_0 - x_h}{2(L_0 - a_0 + x_h)} \tag{15}$$

To study the factors affecting the range of stability, it is easier to shape a number of dimensionless parameters, which contain a wide range of factors in one single parameter. Hence, the following dimensionless parameters are used:

$$\hat{a}_0 = \frac{a_0}{L_0}, \hat{h}_0 = \frac{h_0}{L_0}, \hat{x}_h = \frac{x_h}{L_0}, \hat{x} = \frac{x}{L_0}, \hat{K} = \frac{K}{k_p} \tag{16}$$

and

$$\hat{F} = \frac{F}{k_p L_0} - \frac{h_0}{L_0} \tag{17}$$

In addition, the geometric and stiffness ratios are expressed in the dimensionless form, as follows:

$$\lambda = \frac{\hat{a}_0 - \hat{x}_h}{2(1 - \hat{a}_0 + \hat{x}_h)} \quad and \quad \alpha = \frac{k_n}{k_p} \tag{18}$$

Based on this, Figure 5 can be now obtained by changing the values of the factors that affect the stiffness of the system at different ratios between the geometry and the stiffness. As expected, the best range is achieved when the geometric ratio was equal to the stiffness ratio.

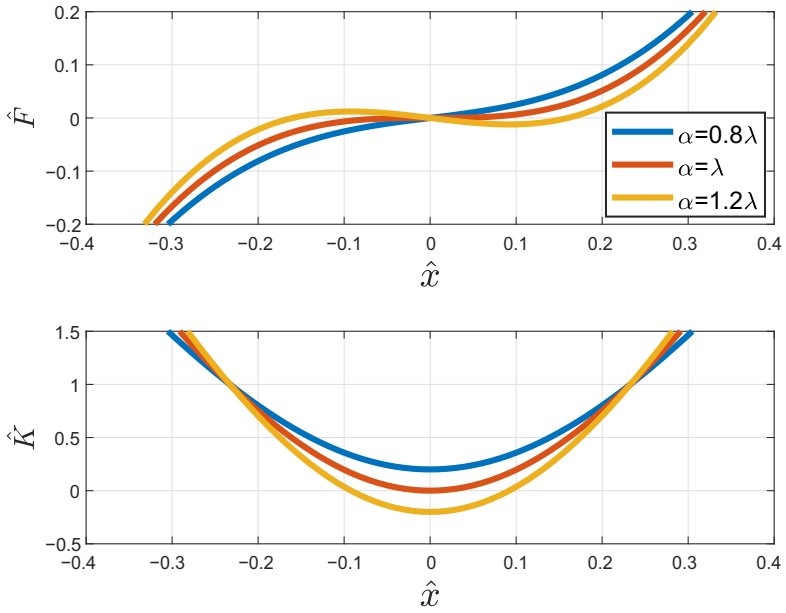


Figure 5. Force and stiffness versus displacement for $\alpha = 0.8\lambda, \alpha = \lambda, \alpha = 1.2\lambda$.

Results shown in Figure 5 lead to defining the best angle of inclination for the oblique springs that achieves the best range of stability (see Figure 6).

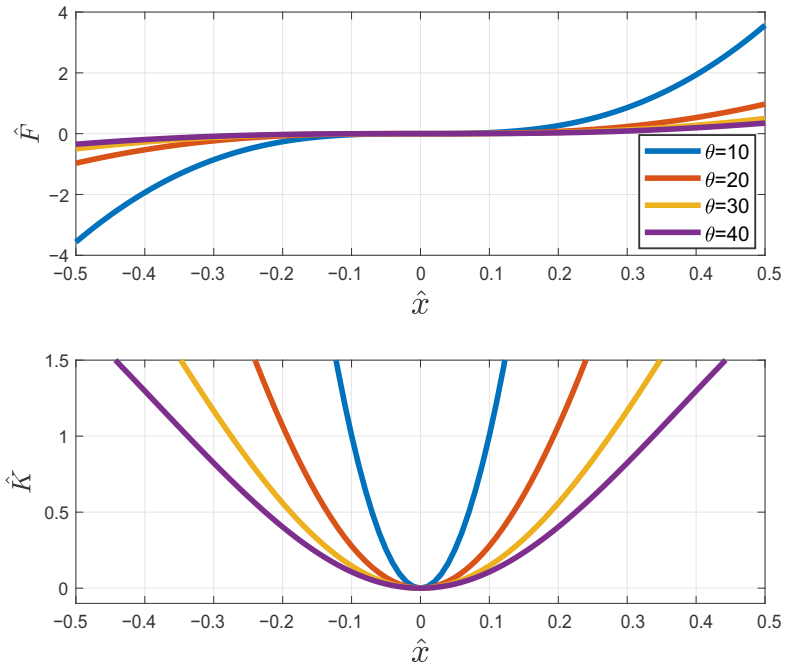


Figure 6. Force and stiffness versus displacement for different oblique angles.

The next step is to find a good approximated representation of the force and stiffness equation. Therefore, a third-order Taylor series is used, as follows:

$$\hat{F} = [1 + 2\alpha(1 - \frac{1}{\hat{a}_0 - \hat{x}_h})]\hat{x} + \frac{\alpha}{(\hat{a}_0 - \hat{x}_h)^3}\hat{x}^3 \tag{19}$$

When the geometric and stiffness ratios are equal, Equation (19) can be reduced as follows:

$$\hat{F} \approx \frac{\alpha}{(\hat{a}_0 - \hat{x}_h)^3}\hat{x}^3 \tag{20}$$

By taking the derivative of the above equation with respect to $\hat{x}$, the dimensionless stiffness parameter may be expressed as

$$\hat{K} \approx \frac{3\alpha}{(\hat{a}_0 - \hat{x}_h)^3}\hat{x}^2 \tag{21}$$

Figures 7 and 8 show that the exact and the approximated solutions are approximately the same, and thus can be used for the analysis discussed in Section 4.

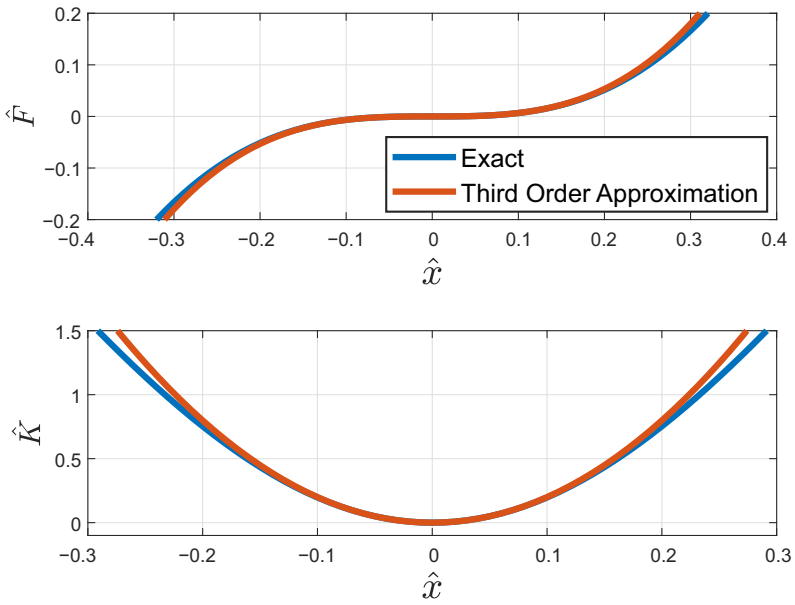


Figure 7. Force and stiffness versus displacement for exact and third-order expressions.

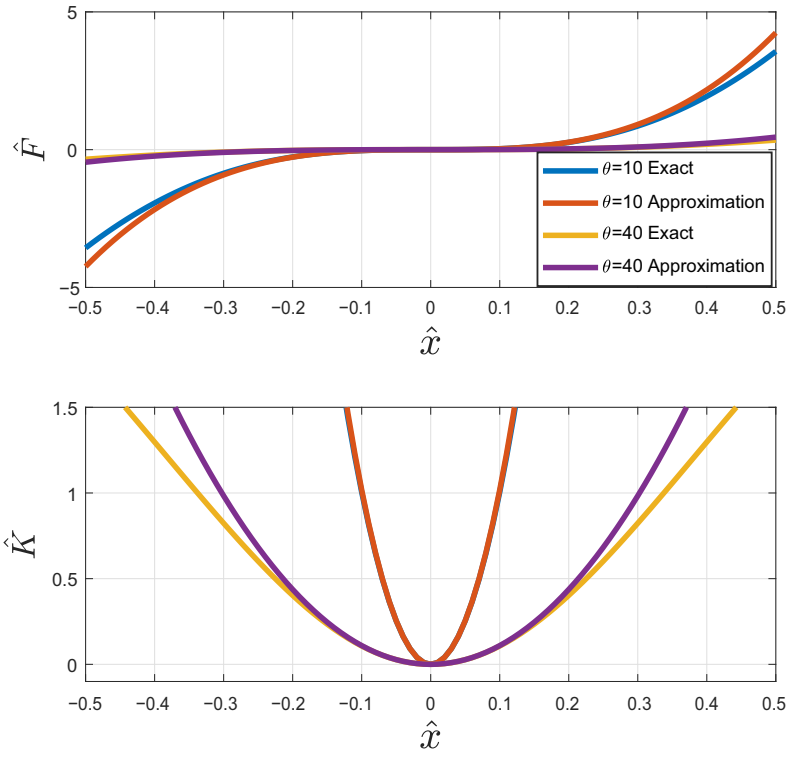


Figure 8. Force and stiffness versus displacement using different oblique angles for exact and third-order expressions.

3.2. Air Spring

This newly modified QZS system becomes very essential because the weight of the driver is not fixed when the driver sits on the seat, which in turn affects the inclination angle of of the oblique springs in the QZS system.

Therefore, the proposed solution for this problem is to introduce an air spring, which can deal with the mass of the driver by inflating or deflating the air spring. In addition, this will help to control the initial position to be at the equilibrium, control the inclination angle of the oblique springs, and finally introduce an adequate amount of damping, which also helps in reducing the force transmitted to the driver.

Remark 1. *Although air spring introduces another stiffness element in the vertical direction, which leads to higher natural frequency and hence less isolation, this amount of stiffness is already present in the vertical spring. Thus, the two systems (the air spring and the vertical spring of the QZS system) will share the same amount of stiffness instead of having a single system, i.e,. nothing has changed in terms of the overall vertical stiffness.*

Remark 2. *It is worth noting that introducing a damper instead of the air spring is not a good solution because obviously having a high amount of damping means losing the opportunity to isolate the system at large frequency ratios. In contrast, the air spring introduces a very small amount of damping and it marginally affects the overall isolation, but majorly isolates the force from being transmitted to the driver.*

In summary, the presence of the air spring is indeed one of the main pillars that this system stands on. It gives the advantage of supporting a variety of loads while keeping the system at the equilibrium position for different types and values of the load. Thus, it achieves the optimum isolation performance without introducing high damping into the system.

4. Numerical Simulation Results

This section consists of two essential parts: the first one proposes an isolator prototype design and selects parameters for each component based on the derived equations in Section 3. The second part is a numerical simulation, which is adopted to verify the authenticity of the proposed isolator theory and its analytical results.

4.1. Prototype Design

In this subsection, the proposed isolator parameters are chosen using the equations that were derived earlier. One of the significant parameters is the geometrical parameter, in which the proposed isolator can fit under the seat. The geometric values of L_0 and a_0 are chosen to be 110 mm and 100 mm, respectively, to fit the system under the drivers' seat of B and C- segment cars [33]. The vertical distance was calculated using the Pythagorean theorem:

$$h_0 = \sqrt{L_0^2 - a_0^2} = \sqrt{110^2 - 100^2} = 45.5 \text{ mm}, \tag{22}$$

consequently,

$$\theta = tan^{-1} = \frac{45.5}{100} = 24.5^\circ \tag{23}$$

As noted in Section 3, the larger oblique angle yields better isolation. However, a larger oblique angle means a longer vertical spring should be chosen, which is not preferred due to the system's size. Therefore, the obtained oblique angle seems a reasonable choice. Assuming that the mass of the seat is 20 kg and the minimum mass of the driver is 40 kg, the stiffness of the vertical spring k_p will equal 12.85 N/mm. Any additional mass over the design mass will be considered by the air spring ($k_{as} \neq 0$). To achieve zero stiffness, the geometric ratio λ must equal the stiffness ratio α, as was shown by Equation (15). The initial horizontal adjustment x_h is set to zero, and the stiffness of the oblique spring k_n will equal 64.22 N/mm.

Figure 9 shows the proposed isolator prototype. The prototype consists of two oblique springs, a vertical spring, an air spring, linear guide rails, upper and lower frame, and two adjustable threads. The adjustable threads are used as horizontal adjustments to ensure that the geometric ratio λ is always equal to the stiffness ratio α, regardless of the load value. In

other words, the adjustable threads are used to increase or decrease the distance x_h based on the load variation, and hence the geometry of the system is altered and the geometric ratio is changed. For this study, the proposed system was tested for specific amounts of load and, consequently, a fixed thread was used (constant x_h), as shown in Figure 9. Hence, for the load variation, it is advisable to use a linear actuator to automatically adjust x_h, as discussed in Section 3. Regarding the load variation, an air spring is used to support any load that exceeds the limit that the vertical spring can support. According to the air spring manufacturer (1M1A-1 Firestone), the relationship between the weight, the pressure, and the stiffness is linear as long as the air spring is used at its recommended design height [34]. Therefore, the air spring is mounted on an inverted U-shaped frame to ensure that when the air spring is inflated with a pressure related to the weight and reached its recommended height, the QZS mechanism will always reach the equilibrium position, thus achieving the optimum isolation. The linear guide rails in the middle are used to guarantee that the movement is only in the z-direction and prevent any bending moment.

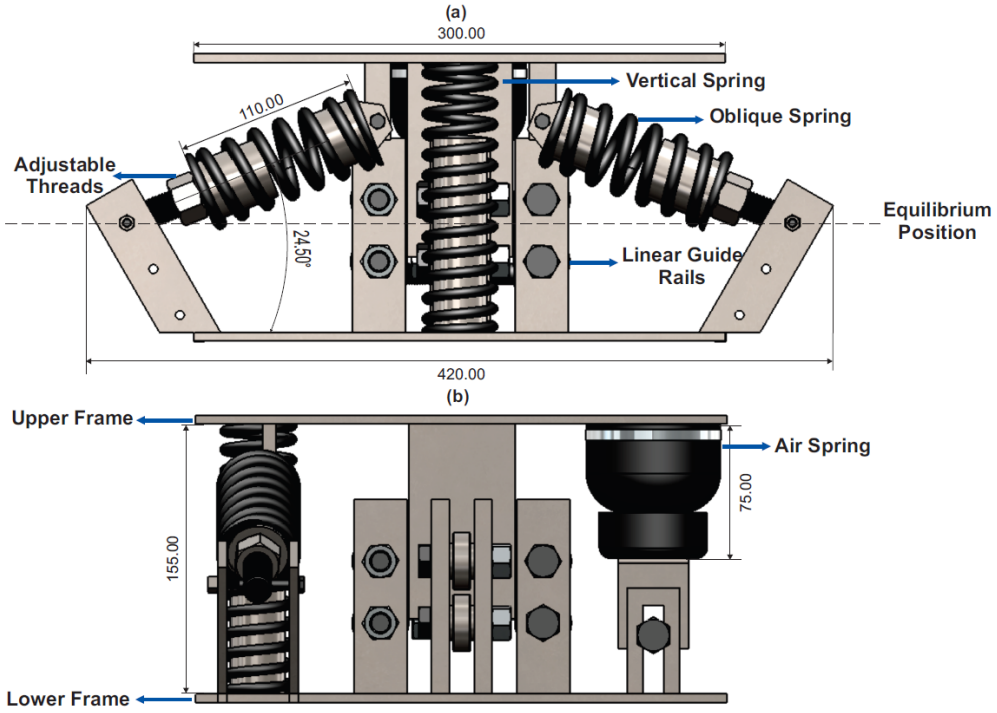


Figure 9. 3D model of the proposed isolator prototype: (**a**) side-view, (**b**) front-view.

The selected parameters of the proposed isolator prototype are shown in Table 1. Note that the mass is the summation of the seat's mass and the driver's minimum expected mass.

Table 1. Selected parameters of the proposed isolator prototype.

k_p (N/mm)	k_n (N/mm)	L_0 (mm)	a_0 (mm)	θ_0 (degree)	m (kg)
12.85	64.22	110	100	24.50	60

Based on the theory and the proposed isolator prototype's theoretical parameters, it can be said with certainty that the prototype exhibits the quasi-zero stiffness behaviour. For further validation, force–displacement and stiffness–displacement curves are introduced. Although the prototype is always at the equilibrium position in the static case, the air spring is an important aspect that should be considered, or it will severely affect the performance. With the load variation, the air amount pumped into the air spring changes depending on the linear relationship noted before; this causes a change in the air spring's stiffness, thus changing the stiffness ratio α. To solve this matter, the geometrical ratio λ

must be changed to a value that equals the new stiffness ratio α_{new} by varying the horizontal adjustment x_h (the only variable in the geometrical ratio equation). Figure 10 shows the force–displacement and stiffness–displacement curves for different loads. The dimensional form of both Equations (20) and (21) are used to produce the results in Figure 10. Note that the horizontal adjustment x_h is not zero at the prototype's design mass due to the air spring initial stiffness that changes the stiffness ratio.

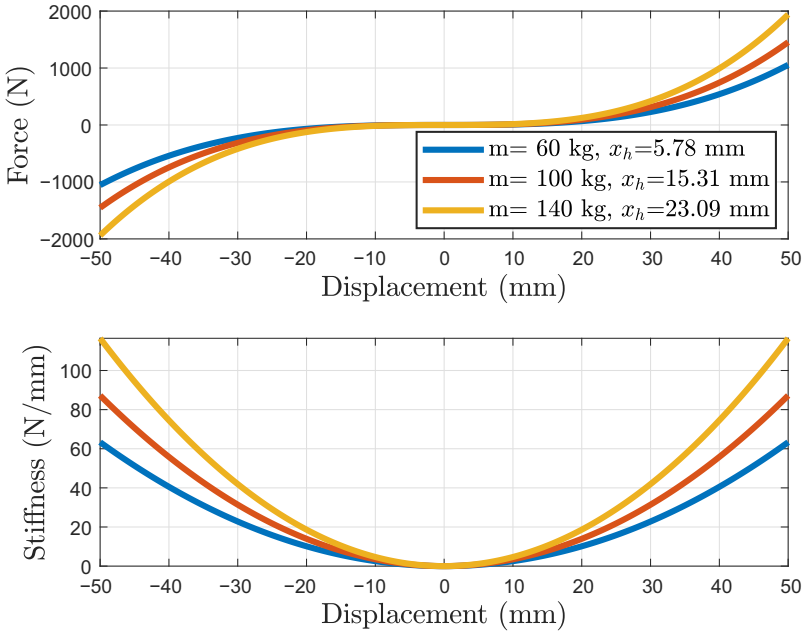


Figure 10. Force–displacement and stiffness–displacement curves for different loads.

4.2. Numerical Simulation

In this subsection, displacement transmissibility is adopted to measure the performance of the proposed system under harmonic excitation. There are three types of tests that may be used to investigate the performance of the proposed system under different amplitudes, damping coefficients, and loads. An equivalent linear mass-spring-damper system is introduced as a comparison to the proposed system in all tests.

The displacement transmissibility results in this section were simulated using MATLAB/Simulink® software. Equation (10) along with Equations (13) and (15) were used to find the values of the geometrical and stiffness parameters needed based on the force acting on the system. Furthermore, a linearization toolbox was used to perform the linear analysis of nonlinear models by assigning the base displacement (d) as an input and the seat displacement (x) as an output.

As noted in Section 3 and according to Equation (11), the natural frequency of the proposed system is not only changing with the chosen parameters but is also changing with the amplitude. Consequently, to verify this point, the effect of increasing the amplitude on the natural frequency is illustrated in Figure 11. Thus, the isolation region is shifted to a larger frequency at a constant load, e.g., $m = 100$ kg. Figure 11 also shows that the damping ratio ζ changes with the natural frequency, which gives an indication for not using a constant ζ. Therefore, in this test, it is assumed that the air spring membrane has a damping coefficient, i.e., $c = 70$ kg/s. Table 2 shows the frequency when the isolation starts (0 dB) at each amplitude. It is good to note that the change in the frequency is linearly proportional to the amplitude, which was given by Equation (11). In contrast, although the amplitude change does not affect the equivalent linear isolator due to its constant natural frequency, it lacks the ability to deal with low frequencies and small amplitudes excitements; this is not the case with the proposed system due to its flexibility.

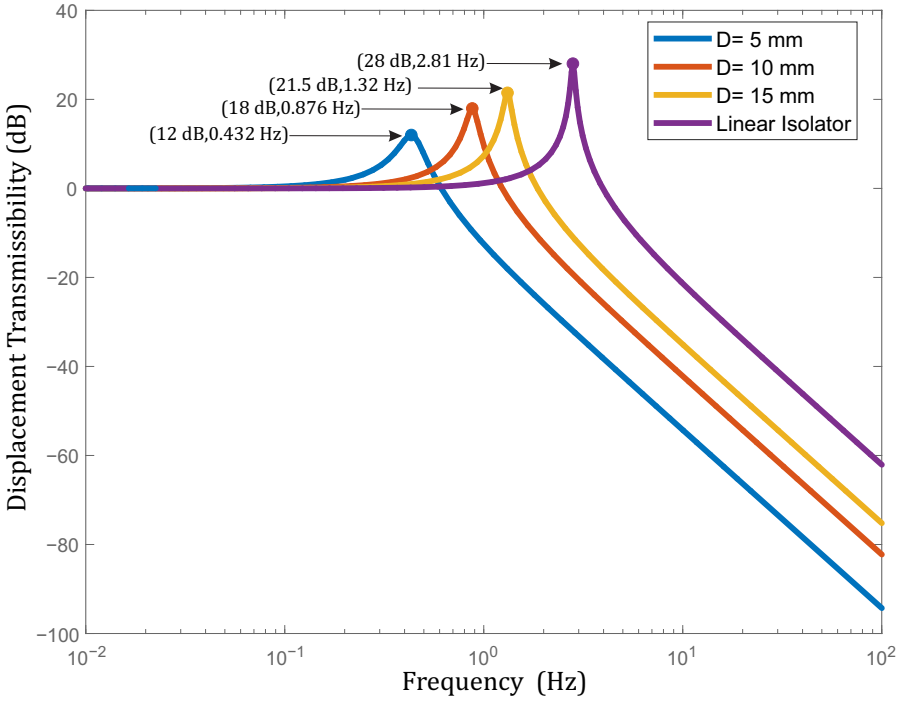


Figure 11. Displacement transmissibility curve under different excitation amplitudes ($m = 100$ kg, and $c = 70$ kg/s).

Table 2. Values for 0 dB frequencies for different amplitudes.

Amplitude (mm)	5	10	15
Frequency (Hz)	0.612	1.24	1.86

It is also imperative to perform tests regarding the damping case, especially in the proposed system, where both of the natural frequency ω_n and the damping coefficient c can change the damping ratio ζ. Figure 12 shows a comparison between the proposed system and the equivalent linear system for different damping coefficients. It can be clearly observed that the proposed system has advantages in the considered aspects, where it has a broader frequency range of the isolation along with the low-peak transmissibility. Table 3 shows the frequency values when the isolation starts (0 dB) at each damping coefficient. It can be noted that the natural frequency ω_n of the proposed system is smaller than the equivalent linear system one. Therefore, this allows the damping ratio ζ to be larger at a constant damping coefficient c and achieving a lower damping frequency ω_d.

Another aspect that cannot be overlooked is the effects of the load variation on performance. Therefore, Figure 13 is used to compare performance of the proposed system and the equivalent linear system at different loads. Similar to the previous test, the proposed system has better isolation and lower peak transmissibility. It is noted that the equivalent linear isolator has a big deflection due to the added load, which has a force value that is larger than the vertical spring force k_p. In contrast, the proposed system keeps the load at the equilibrium position thanks to the air spring. Table 4 shows the frequency when the isolation starts (0 dB) at each load. It can also be seen that although the vertical stiffness (k_p and k_{as}) of the proposed system is larger than the linear isolator stiffness (k_p only), it still yields good results.

Table 3. Values for 0 dB frequencies at different damping coefficients.

Damping coefficient (kg/s)		50	350
Frequency (Hz)	Proposed	1.24	1.11
	Linear	3.97	3.93

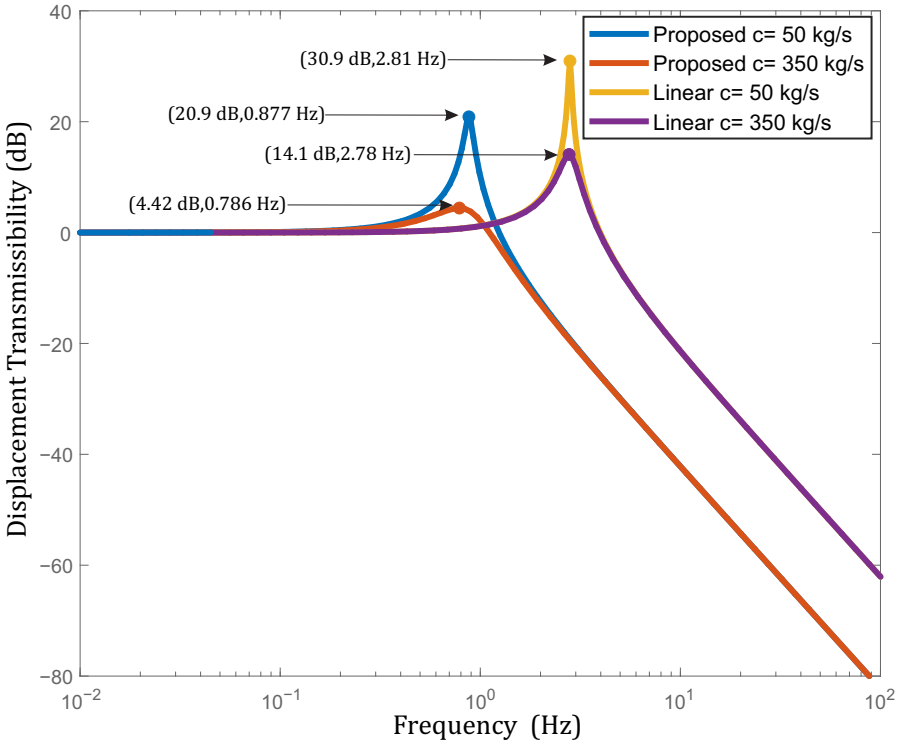


Figure 12. Displacement transmissibility curve for different damping coefficients ($D = 10$ mm, and $m = 100$ kg).

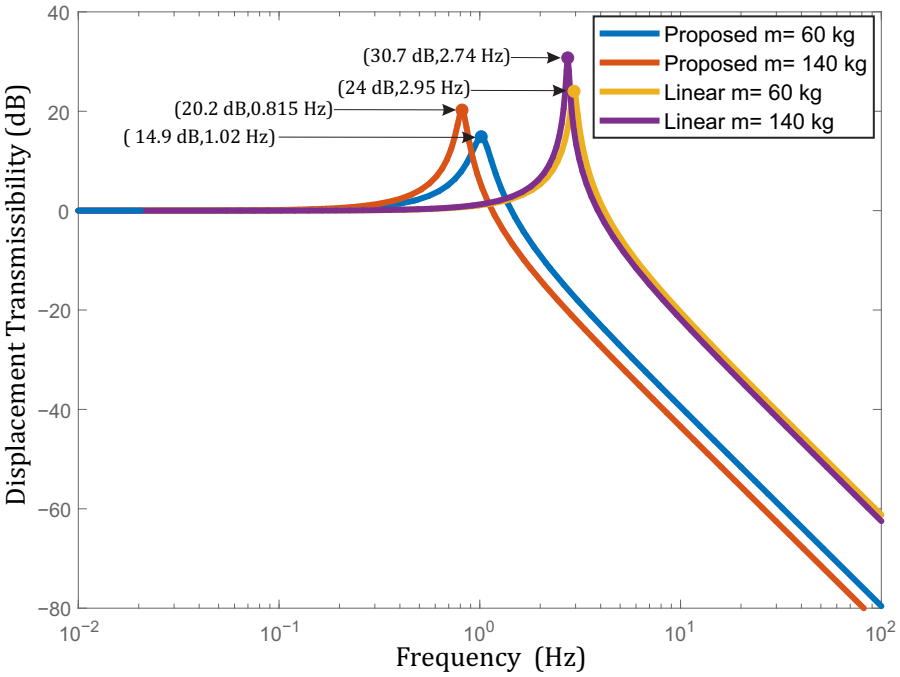


Figure 13. Displacement transmissibility curve for different damping loads ($D = 10$ mm, and $c = 70$ kg/s).

Table 4. Values for 0 dB frequencies at different loads.

Load (kg)		60	140
Frequency (Hz)	Proposed	1.44	1.15
	Linear	4.17	3.88

5. Conclusions

This study has focused on isolating harmful low-frequency vibrations that are transmitted to the vehicle's seat. The solution is based on lowering the natural frequency of the system by introducing an isolation system with low or zero dynamic stiffness, and thus, the frequency range of isolation will be increased.

The practical implementation for the proposed vibration isolation system is based on implementing a simple and compact system that combines the merits of the QZS with an air spring, which is able to isolate extremely low levels of vibrations. Herein, the novelty of the proposed system is (i) its capability of isolating the unpredictable roadway low-level disturbances and (ii) its compatibility with B-segment and C-segment cars, which are considered important factors for the future of passenger car production.

Parametric analyses were performed to prove the efficiency of the proposed system in terms of the displacement transmissibility (a pointer of efficiency). Displacement transmissibility was tested under different amplitudes of excitation, different driver loads, and different damping coefficients. For each test, a comparison was generated between the proposed system and an equivalent linear mass-spring-damper system. The results have revealed that the proposed system was very efficient and better than the equivalent linear system under all circumstances. It was also observed that the proposed system provides lower peak transmissibility and a broader range of frequency isolation. More specifically, the proposed system was able to isolate vibrations at very low frequencies of excitation down to 0.65 Hz. Thus, for different conditions of excitation amplitudes and driver loads, the range of frequency of isolation was still suitable at less than 1.85 Hz.

Future research efforts will be dedicated to the implementation of the proposed system to perform experimental tests to verify the system performance compared with the simulation results. Finally, further studies are required to explore the effects of the air spring pressure, airflow, inflation, and deflation control for the isolator efficiency.

Author Contributions: Conceptualization, methodology, investigation, and original draft preparation: M.A. (Mohammad Abuabiah), Y.D., L.H. and I.H.A.; review and editing: M.A. (Mohammad Abuabiah), L.H., I.H.A.,Y.D. and M.A. (Mahmoud Assad); supervision: P.P. and M.A. (Mohammad Abuabiah); project administration and funding acquisition: P.P. All authors have read and agreed to the published version of the manuscript.

Funding: This research received no external funding.

Institutional Review Board Statement: Not applicable.

Informed Consent Statement: Not applicable.

Data Availability Statement: Not applicable.

Acknowledgments: The authors would like to thank the Mechanical and Mechatronics Engineering Departments at An-Najah National University for providing access to their labs for executing data analysis. Sincere thanks are also extended to the University of Luxembourg for its continuous support.

Conflicts of Interest: The authors declare no conflict of interest.

References

1. Velmurugan, P.; Kumaraswamidhas, L.; Sankaranarayanasamy, K. Whole body vibration analysis for drivers of suspended cabin tractor semitrailer. *Exp. Tech.* **2014**, *38*, 47–53. [CrossRef]
2. Pazooki, A.; Cao, D.; Rakheja, S.; Boileau, P.É. Ride dynamic evaluations and design optimisation of a torsio-elastic off-road vehicle suspension. *Veh. Syst. Dyn.* **2011**, *49*, 1455–1476. [CrossRef]
3. Rakheja, S.; Stiharu, I.; Zhang, H.; Boileau, P.É. Seated occupant interactions with seat backrest and pan, and biodynamic responses under vertical vibration. *J. Sound Vib.* **2006**, *298*, 651–671. [CrossRef]
4. DeShaw, J.; Rahmatalla, S. Predictive discomfort and seat-to-head transmissibility in low-frequency fore-aft whole-body vibration. *J. Low Freq. Noise Vib. Act. Control* **2011**, *30*, 185–195. [CrossRef]
5. Mansfield, N.J.; Mackrill, J.; Rimell, A.N.; MacMull, S.J. Combined effects of long-term sitting and whole-body vibration on discomfort onset for vehicle occupants. *Int. Sch. Res. Not.* **2014**, *2014*, 852607. [CrossRef]
6. Dewangan, K.; Rakheja, S.; Marcotte, P. Gender and anthropometric effects on whole-body vibration power absorption of the seated body. *J. Low Freq. Noise Vib. Act. Control* **2018**, *37*, 167–190. [CrossRef]
7. Wang, W.; Rakheja, S.; Boileau, P.É. Effects of sitting postures on biodynamic response of seated occupants under vertical vibration. *Int. J. Ind. Ergon.* **2004**, *34*, 289–306. [CrossRef]
8. Wang, W.; Rakheja, S.; Boileau, P.É. Effect of back support condition on seat to head transmissibilities of seated occupants under vertical vibration. *J. Low Freq. Noise Vib. Act. Control* **2006**, *25*, 239–259. [CrossRef]
9. Bhiwapurkar, M.; Saran, V.; Harsha, S. Effects of posture and vibration magnitude on seat to head transmissibility during exposure to fore-and-aft vibration. *J. Low Freq. Noise Vib. Act. Control* **2019**, *38*, 826–838. [CrossRef]
10. Gan, Z.; Hillis, A.J.; Darling, J. Adaptive control of an active seat for occupant vibration reduction. *J. Sound Vib.* **2015**, *349*, 39–55. [CrossRef]
11. Li, C.; Liang, M.; Wang, Y.; Dong, Y. Vibration suppression using two-terminal flywheel. Part II: application to vehicle passive suspension. *J. Vib. Control* **2012**, *18*, 1353–1365. [CrossRef]
12. Zhang, M.; Xu, F. Tuned mass damper for self-excited vibration control: Optimization involving nonlinear aeroelastic effect. *J. Wind Eng. Ind. Aerodyn.* **2022**, *220*, 104836. [CrossRef]
13. Stein, G. A driver's seat with active suspension of electro-pneumatic type. *J. Vib. Acoust.* **1997**, *119*, 230–235. [CrossRef]
14. Maciejewski, I.; Meyer, L.; Krzyzynski, T. The vibration damping effectiveness of an active seat suspension system and its robustness to varying mass loading. *J. Sound Vib.* **2010**, *329*, 3898–3914. [CrossRef]
15. Ning, D.; Sun, S.; Li, H.; Du, H.; Li, W. Active control of an innovative seat suspension system with acceleration measurement based friction estimation. *J. Sound Vib.* **2016**, *384*, 28–44. [CrossRef]
16. Ning, D.; Sun, S.; Du, H.; Li, W.; Zhang, N. Vibration control of an energy regenerative seat suspension with variable external resistance. *Mech. Syst. Signal Process.* **2018**, *106*, 94–113. [CrossRef]
17. Choi, S.B.; Nam, M.H.; Lee, B.K. Vibration control of a MR seat damper for commercial vehicles. *J. Intell. Mater. Syst. Struct.* **2000**, *11*, 936–944. [CrossRef]
18. Watkins, D. Scissor Lift Mechanism. US Patent 6,679,479, 20 January 2004.
19. Carrella, A.; Brennan, M.; Waters, T.; Shin, K. On the design of a high-static–low-dynamic stiffness isolator using linear mechanical springs and magnets. *J. Sound Vib.* **2008**, *315*, 712–720. [CrossRef]
20. Zhou, N.; Liu, K. A tunable high-static–low-dynamic stiffness vibration isolator. *J. Sound Vib.* **2010**, *329*, 1254–1273. [CrossRef]
21. Zheng, Y.; Zhang, X.; Luo, Y.; Yan, B.; Ma, C. Design and experiment of a high-static–low-dynamic stiffness isolator using a negative stiffness magnetic spring. *J. Sound Vib.* **2016**, *360*, 31–52. [CrossRef]
22. Dong, G.; Zhang, X.; Xie, S.; Yan, B.; Luo, Y. Simulated and experimental studies on a high-static-low-dynamic stiffness isolator using magnetic negative stiffness spring. *Mech. Syst. Signal Process.* **2017**, *86*, 188–203. [CrossRef]
23. Kovacic, I.; Brennan, M.J.; Waters, T.P. A study of a nonlinear vibration isolator with a quasi-zero stiffness characteristic. *J. Sound Vib.* **2008**, *315*, 700–711. [CrossRef]
24. Carrella, A.; Brennan, M.; Kovacic, I.; Waters, T. On the force transmissibility of a vibration isolator with quasi-zero-stiffness. *J. Sound Vib.* **2009**, *322*, 707–717. [CrossRef]
25. Xu, D.; Yu, Q.; Zhou, J.; Bishop, S. Theoretical and experimental analyses of a nonlinear magnetic vibration isolator with quasi-zero-stiffness characteristic. *J. Sound Vib.* **2013**, *332*, 3377–3389. [CrossRef]
26. Liu, X.; Huang, X.; Hua, H. On the characteristics of a quasi-zero stiffness isolator using Euler buckled beam as negative stiffness corrector. *J. Sound Vib.* **2013**, *332*, 3359–3376. [CrossRef]
27. Zhou, J.; Wang, X.; Xu, D.; Bishop, S. Nonlinear dynamic characteristics of a quasi-zero stiffness vibration isolator with cam–roller–spring mechanisms. *J. Sound Vib.* **2015**, *346*, 53–69. [CrossRef]
28. Kim, K.R.; You, Y.h.; Ahn, H.J. Optimal design of a QZS isolator using flexures for a wide range of payload. *Int. J. Precis. Eng. Manuf.* **2013**, *14*, 911–917. [CrossRef]
29. Ahn, K.K. Active pneumatic vibration isolation system using negative stiffness structures for a vehicle seat. *J. Sound Vib.* **2014**, *333*, 1245–1268.
30. Zou, W.; Cheng, C.; Ma, R.; Hu, Y.; Wang, W. Performance analysis of a quasi-zero stiffness vibration isolation system with scissor-like structures. *Arch. Appl. Mech.* **2021**, *91*, 117–133. [CrossRef]

31. Liao, X.; Zhang, N.; Du, X.; Zhang, W. Theoretical modeling and vibration isolation performance analysis of a seat suspension system based on a negative stiffness structure. *Appl. Sci.* **2021**, *11*, 6928. [CrossRef]
32. Lepine, J.; Rouillard, V.; Sek, M. Review paper on road vehicle vibration simulation for packaging testing purposes. *Packag. Technol. Sci.* **2015**, *28*, 672–682. [CrossRef]
33. Kamp, I. The influence of car-seat design on its character experience. *Appl. Ergon.* **2012**, *43*, 329–335. [CrossRef] [PubMed]
34. Firestone Industrial Products. *Airstroke Actuators Airmount Isolators: Engineering Manual and Design Guide*, Metric ed.; Middlesex: London, UK, 1997.